Giant doping response of magnetic anisotropy in MnTe

Duncan H. Moseley, Keith M. Taddei, Jiaqiang Yan, Michael A. McGuire, Stuart Calder, M.
M. H. Polash, Daryoosh Vashaee, Xiaofan Zhang, Huaizhou Zhao, David S. Parker, Randy
S. Fishman, and Raphaël P. Hermann

Giant Doping Response of Magnetic Anisotropy in MnTe

Duncan H. Moseley,[1] Keith M. Taddei,[2] Jiaqiang Yan,[1] Michael A. McGuire,[1]
Stuart A. Calder,[2] M. M. H. Polash,[3,4] Daryoosh Vashaee,[3,4] Xiaofan Zhang,[5]
Huaizhou Zhao,[5] David S. Parker,[1] Randy S. Fishman,[1] and Raphaël P. Hermann[1]

[1]*Materials Science and Technology Division, Oak Ridge National Laboratory, Oak Ridge, TN 37831, USA*
[2]*Neutron Scattering Division, Oak Ridge National Laboratory, Oak Ridge, TN 37831, USA*
[3]*Department of Electrical and Computer Engineering,*
North Carolina State University, Raleigh, NC 27606, USA
[4]*Department of Materials Science and Engineering,*
North Carolina State University, Raleigh, NC 27606, USA
[5]*Beijing National Laboratory for Condensed Matter Physics,*
Institute of Physics, Chinese Academy of Sciences, Beijing 100190, China

Developing simple ways to control spin states in spintronic devices is a crucial step towards increasing their functionality. MnTe is a room-temperature antiferromagnet with promising spintronic properties, including thermospintronics and magnon-based devices. Here, we show that, in MnTe, less than 1% Li is sufficient to produce a dramatic spin reorientation as observed by neutron diffraction. The behavior of the 0001 magnetic Bragg peak reveals a significant reorientation of the Mn spins from planar in the pure material to almost completely axial with minimal Li-doping. Temperature dependence of the magnetic peaks in Li-doped samples indicates that axial spins shift back to planar suddenly upon approaching the Néel temperature ($T_N = 307$ K). Density functional theory (DFT) calculations support the idea that a shift in the Fermi level caused by doping is responsible for switching the material between two competing magnetic ground states. These results pave the way for developing easy switching of magnetic states in functional materials such as spintronic devices and topological insulators.

I. INTRODUCTION

Controlling reorientation of spins is critical for spintronic and information technologies[1–3]. This is especially important for future antiferromagnetic (AFM) spintronic devices, which are advantageous compared to ferromagnetic materials due to their absence of stray fields, insensitivity to parasitic magnetic fields, and ultrafast dynamic response[4, 5]. Spin reorientation typically requires the application of strain,[6–8] large magnetic fields, or interfacing with other magnetic materials,[9] among other methods[10]. Developing efficient means to control the direction of magnetic moments in AFM materials is key to advancing this field. Additionally, the spin orientation can affect thermodynamics properties[11, 12].

MnTe is an AFM *p*-type semiconductor with a Néel temperature (T_N) of 307 K, with NiAs structure[13, 14] of alternating hexagonal layers of Mn and Te (space group $P6_3/mmc$) with each Mn^{2+} tetracoordinated to four Te^{2-} ions. In close proximity to T_N, MnTe shows a pronounced increase in thermopower,[15] suggesting coupling between magnetic and electronic degrees of freedom. Excess thermopower in the paramagnetic state[16] suggests that local thermal fluctuations of the magnetization give rise to a paramagnetic spin-Seebeck[17, 18] effect similar to that in ferromagnets,[19] thus also exhibiting thermospintronics potential.

MnTe has garnered considerable attention for its utility as a binary[20] thermoelectric[21, 22] material, potential spintronic applications,[4, 23] and usefulness as an ultra-responsive photodetector when grown as a thin film[24, 25]. AFM spintronic devices exhibit unique properties, such as stability against external magnetic fields and nonvolatility. The ability to manipulate size, orientation, and ordering of the magnetic moments is key for such devices, such as spin valves, where resistivity can be controlled by the spin orientation of the layers[2]. Such manipulation is achievable, e.g., by current-induced magnetic torques,[26] the inverse spin galvanic effect,[27] and by either field cooling through T_N or applying high magnetic fields in the AFM state to alter domain populations[28, 29]. Tuning the spin direction could also provide control on spin texture in material deposited on MnTe[30, 31].

Recently, MnTe has found use in topological insulators such as the layered van der Waals heterostructure $MnBi_2Te_4$,[32–40] comprised of alternating layers of MnTe and Bi_2Te_3. Additionally, MnTe has a band gap of 1.27 to 1.46 eV,[13, 29] which can be used to exchange-bias topological insulators or metals. $(Bi,Sb)_2Te_3$ has been grown on MnTe and exhibited exchange-bias at the interface, which enabled tuning of the topological charge[41]. Consequently, controlling the band structure, Fermi level, and spin direction of MnTe may open novel directions for spintronic and other transport applications.

The spin dynamics of MnTe was studied by inelastic neutron scattering in the ordered phase[42] and in the paramagnetic regime[16]. The latter work revealed a liquid-like spin-spin relaxation in Li-doped MnTe with a width of ∼25 meV. Neutron diffraction was used to determine MnTe to be an easy-plane material,[43]. The

magnetic anisotropy in MnTe films can be manipulated by strain when choosing a specific substrate material[44]. This is in contrast to layered $MnBi_2Te_4$, which possesses a similar magnetic structure with axial Mn spins[45] and an internal heterostructure with large strain that promotes the formation of Bi_{Mn} antisite defects, which significantly shift the Fermi level[38].

Theoretical work has largely focused on the electronic structure and magnetic properties of MnTe[44, 46, 47]. Phonons in MnTe do not strongly couple to magnetism, which prevents phonons from degrading the magnon mean-free-path[48]. This weak coupling may prove beneficial in magnon-based spintronic devices.

A recent work examined the effect of hole-doping on $Fe_{3-x}GeTe_2$, which produced a very clear modulation of the magnetic anisotropy, however the system required a doping level of $x = 36\%$[49]. Tuning of the magnetic anisotropy and causing spin reorientation via doping typically requires large amounts of dopants to achieve a significant effect and can lead to intermediate states between the planar and axial phases or result in a gradual shift between phases[38, 50–56].

Here, we present neutron powder diffraction measurements and density functional theory (DFT) calculations on pure and Li-doped MnTe. In recent work[16], Li was chosen as a dopant that enhances the thermoelectric properties by paramagnon drag. Here we investigate the impact of doping on the magnetic structure. Our results indicate that MnTe exhibits competing magnetic ground states that enable easy tuning of the spin orientation. Doping with as little as 0.3% Li is sufficient to shift the Fermi level and achieve a swift spin reorientation from planar to axial that survives up to ∼250 K. Because this effect is driven by moving the Fermi level this effect is likely not specific to Li as a dopant.
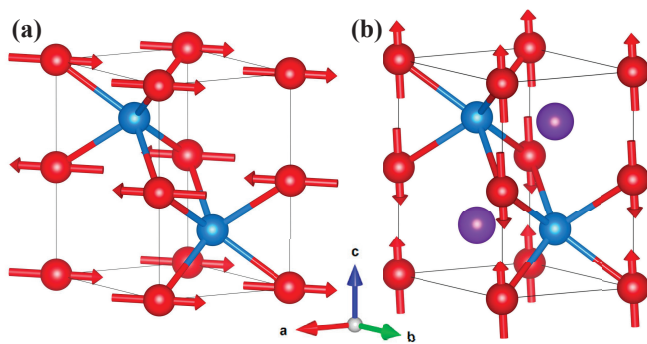

FIG. 1: Magnetic structure of pure MnTe showing in-plane (a) versus axial (b) spins in the 5% Li-doped analogue. Atoms are represented by red (Mn), blue (Te), and purple (Li).

II. EXPERIMENTAL SECTION

Synthesis

Single crystals of MnTe (**1**) were grown out of Te flux. Reduced Mn pieces and Te shot were mixed in the molar ratio of Mn:Te = 36:64, placed in a 2 mL Canfield crucible, and sealed under vacuum in a silica ampoule. The sealed ampoule was kept at 890 °C for 12 days, after which the Te flux was separated from crystals by decanting. X-ray powder diffraction of pulverized crystals found no impurity phase.

Powdered MnTe (**2**) was synthesized by combining elemental Mn and Te in a 1:1 molar ratio in an alumina crucible. The crucible was sealed under vacuum inside a fused silica ampoule, heated to 900 °C over 9 hours, and held there for 24 hours before turning off the furnace and allowing it to cool naturally. The reaction product was then ground into a powder, placed in an alumina crucible, and sealed under vacuum in a fused silica ampoule. The ampoule was heated to 925 °C over a few hours, held at this temperature for three days, and then quenched in ice water. X-ray diffraction showed the final product to be nearly phase pure MnTe, with 3 wt. % $MnTe_2$ determined by Rietveld refinement.

Further samples (**3-7**) with nominal compositions of $Mn_{1-x}Li_xTe$ ($x = 0\%$, 0.3%, 1%, 3%, 5%) were synthesized by ball milling the raw elements (Mn powder, 99.99%; Li chunks, 99.9%; Te chunks, 99.999%) within an argon-filled stainless steel jar using a high-energy ball-milling machine (SPEX 8000D). The materials were milled for 8 hours and hot pressed at 1173 K for 20 min by spark plasma sintering under axial pressure of 40 MPa with a heating rate of 50 K/min[7]. The densities of the obtained samples were not less than 97% relative to the theoretical values. Refinement of the Mn and Te occupancy indicated samples **1-3** were slightly Mn-rich. A minor ($< 2\%$) MnO impurity is present in several of these samples, as determined by neutron diffraction. The MnO impurity has no effect on the spin orientation of MnTe as it exists as a separate phase. Whereas the solubility limit of Li in MnTe is ∼9%,[57] the actual incorporated Li % is likely lower than the nominal amount in each sample as some Li will segregate outside the MnTe lattice. However, there is a clear trend in the lattice constants with increased doping, see Supplementary Figure 3,[58] which can be compared with literature[57] to qualitatively determine how much Li is incorporated.

Magnetic Susceptibility

Magnetization measurements of **1**, **2**, **4**, **5**, and **7** were collected on cooling in a 1 kOe static field using a Quantum Design Magnetic Property Measurement System (DC SQUID magnetometer). These measurements

reveal a transition between 45 and 85 K in pure and Li-doped MnTe, similar to that seen previously,[59] see Supplementary Figure 1[58]. However, while this transition is not well understood, it does not appear to be tied to the magnetic moment orientation and is thus not the focus of this work.

Neutron Scattering

Neutron powder diffraction was performed using the HB-2A powder diffractometer at the High Flux Isotope Reactor (HFIR), Oak Ridge National Laboratory (ORNL)[60]. A germanium monochromator was used to select a wavelength of 2.41 Å from the Ge(113) reflection. The samples were each loaded into Al cans. Data was collected from 4 to 300 K using a closed cycle refrigerator (CCR) and up to 360 K using a high-temperature sample stick. Symmetry-allowed magnetic structures were considered using both representational analysis with SARAh[61] and magnetic space groups with the Bilbao Crystallographic Server[62]. Rietveld refinements were performed using Fullprof[63].

Inelastic neutron scattering (INS) was performed using the ARCS beamline at the Spallation Neutron Source (SNS), ORNL[64] on a powder sample of the 3% Li-doped MnTe (**6**) contained in an aluminum sample can. Data were collected using a 60 meV incident neutron energy. "Diffraction" data were extracted as a scattering function $S(Q)$ integrated over an energy range of -2 to 2 meV.

Calculations

DFT calculations (GGA+U+SOC, U = 5 eV)[65] were performed within the c-axis nearest neighbor magnetic structure for two orientations of Mn spin moments: (001) and (110).

III. RESULTS AND DISCUSSION

Powder Neutron Diffraction

We collected diffractograms of seven samples of Li-doped and pure MnTe (see structures in Figure 1) on the HB-2A neutron powder diffractometer. The obtained lattice constants are listed in Table 1 with the sample type, lattice parameters, and Li %. One sample (**6**) was rejected as an outlier as all data indicated the incorporated Li was significantly less than the nominal 3%. Data pertaining to this sample is presented in the Supplementary Material[58].

The introduction of Li causes a large effect on the canting of the Mn spins and diffraction pattern, however the effect on structural peaks is small. To determine where

the Li ions reside in the lattice, we tried refinements with Li on every Wyckoff position in the $P6_3/mmc$ space group. The 2d position yielded the best fit within the model, signaling that Li resides on an interstitial site, forming a trigonal bipyramid with the Te residing on the 2c site, see Figure 1.

Whereas neutrons are vital to visualizing the spins of a material, only the magnetization component ($M_{\perp Q}$) perpendicular to the scattering vector Q contributes magnetic scattering. Pure MnTe exhibits a strong 0001 structurally-forbidden magnetic peak below T_N = 307 K at Q = 0.94 Å^{-1}, see Figure 2. The magnetic peak intensity here is significant as the magnetic moment is purely in-plane (see Figure 1) and Q is aligned along c. The intensity of this peak is therefore a direct indicator of $M_{\perp c}$, assuming the magnetic moment remains relatively constant among different samples. Thus, pure and Li-doped samples are easy to distinguish since the 0001 peak has significant intensity for the pure samples but is vanishingly weak in the doped samples.
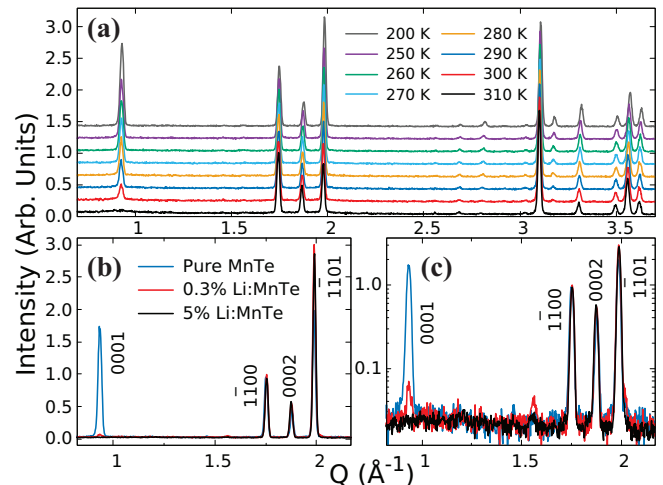

FIG. 2: (a) Temperature dependence of the neutron diffraction of pure MnTe (**1**) from 200 to 310 K. (b-c) Neutron powder diffraction of MnTe at 150 K with Li doping levels of 0%(**1**), 0.3%(**4**), and 5%(**7**) presented in linear (b) and logarithmic (c) scales. All data sets were scaled to match the Q = 1.76 Å^{-1} peak intensity.

The magnetic peak intensities decrease with increasing temperature according to a power law until reaching zero intensity at T_N = 307 K, see Supplemental Figure 2[58]. Two other purely magnetic peaks with similar behaviour are the 0003 and $2\bar{1}\bar{1}1$ at Q = 2.83 Å^{-1} and 3.19 Å^{-1}, respectively. In contrast, the purely structural peak $1\bar{1}00$ at Q = 1.76 Å^{-1} does not show any intensity change with temperature beyond what is expected from the decreasing Debye-Waller factor. A calculation of the structure factor of this peak shows it is not significantly affected by Li-doping and does not get a contribution from magnetism. Both of these characteristics are found

TABLE I: Nominal lithium content, sample type, and lattice parameters at 4 and 290 K for each MnTe sample.

Sample	Li %	Type	a_{4K}	a_{290K}	c_{4K}	c_{290K}	c/a_{4K}	c/a_{290K}
1	0	Crushed SC	4.12085(5)	4.14147(7)	6.6504(1)	6.7007(2)	1.6138	1.6180
2	0	Powder	4.12161(5)	4.14215(7)	6.6517(1)	6.7013(2)	1.6139	1.6178
3	0	Pellet	4.115742(5)	4.13778(5)	6.6607(1)	6.7047(1)	1.6183	1.6204
4	0.3	Pellet	4.11422(8)	4.1364(1)	6.6622(2)	6.7042(3)	1.6195	1.6212
5	1	Pellet	4.11354(4)	4.13621(6)	6.6658(1)	6.7076(1)	1.6204	1.6216
6[a]	3	Pellet	4.11530(4)	4.1381(1)	6.6620(1)	6.7027(3)	1.6188	1.6203
7	5	Pellet	4.10790(4)	4.1309(1)	6.6575(2)	6.6996(3)	1.6207	1.6214

[a] [a]See discussion of this sample in SM, as actual Li content was found to be lower than 3%.
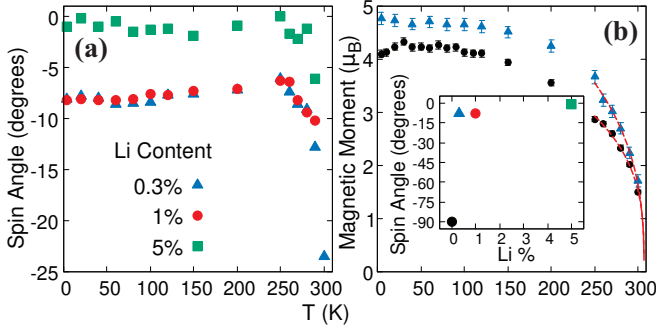

FIG. 3: (a) Magnetic moment of pure (**1**, black circles) and 0.3% Li-doped (**4**, blue triangles). (b) Spin angle (relative to the c-axis) of the four Li-doped samples as a function of temperature. (Inset) Spin angle vs. Li-content at 4 K. The spin angle error is on the order of 2°.

in other peaks, including $1\bar{1}01$ ($Q = 2.00$ Å^{-1}) and $20\bar{2}1$ ($Q = 3.65$ Å^{-1}), with magnetic intensity superposed on the nuclear intensity that does not exhibit significant intensity change at T_N. As the temperature increases, the magnetic intensity decreases until $T_N = 307$ K, at which point the peaks are purely structural. Thus, these peaks contain a magnetic contribution below T_N.

Upon doping with Li, as little as 0.3%, the intensity of the magnetic 0001 peak at 4.2 K decreases significantly. With larger Li doping, up to 5%, the 0001 peak vanishes as the moment almost fully aligns with the new easy-axis. In contrast, Li-doping leads to an increase in intensity of the mixed magnetic/structural $1\bar{1}01$ peak at $Q = 2.00$ Å^{-1}. Purely structural peaks in Li-doped samples exhibit similar behavior to the pure MnTe samples and show only weak, Debye-Waller factor related, intensity changes with temperature. The 0001 peak vanishing indicates the spin reorientation is a volume effect instead of localized around the interstitial Li ions. If only the spins around the doping site reoriented, then a substantial peak would remain at such low dopant %.

To characterize the magnetic order, we used representational theory (as implemented in SARAh). The magnetic peaks can be indexed without any change to the nuclear unit cell, indicating a k vector $k = (000)$. $k =$

0 in the $P6_3/mmc$ space group for the 2a Wyckoff position allows four possible irreducible representations, as shown in Supplementary Table 1[58]. We systematically tried all possible structures and found that basis vectors (BV) ψ_5 and ψ_6 in the Γ_{11} irrep provide the best fits for the parent compound describing an in-plane AFM structure (see ψ_5 in Figure 1a). Powder neutron diffraction is not able to choose between these basis vectors as both provide identical fits and moments. However, the in-plane moment orientation was previously determined to lie along the $1\bar{1}00$ direction,[44] which is equivalent to the ψ_6 BV (magnetic space group No. 63.462, $Cm'c'm$) with the magnetic moment perpendicular to the b axis. In a strongly ionic material such as MnO, where the O is highly electronegative, the Mn is spin-only with a quenched half-filled shell. Te is much less electronegative than O, so we expect the moment to be slightly decreased as some electron density remains, which likely deviates from the full $S = 5/2$ spin-only moment[66].

Upon Li-doping the magnetic scattering noticeably changes (as described above) and analysis requires a second basis vector (ψ_2 in the Γ_7 irrep). In this model (magnetic space group No. 63.464, $Cm'cm'$), the magnetic moments cant significantly out of the ab plane (Figure 1b). These models were incorporated into the Rietveld refinement of each compound (using *Fullprof*) with pure samples using a single BV and irrep and Li-doped samples using two. This model proves adequate for higher Li doping. The incorporation of two separate BVs suggests MnTe may possess two competing magnetic ground states, where ψ_5 is marginally dominant in the pure material, and ψ_2 quickly becomes dominant upon doping. These two states are likely almost degenerate, and doping as little as 0.3% is enough to establish ψ_2 as the ground state. As the Li concentration increases, the low-temperature spin angle approaches an axial orientation. The temperature-dependent transition in pure MnTe is second-order since there is no reorientation of the spins[42]. Landau theory states that second-order transitions involve the build-up of magnetic fluctuations that have the symmetry of only a single BV[67]. Hence, the phase transition as a function of doping cannot be second order as both orientations are described by different BVs and the canted orientations are simply combi-

nations of these BVs. This suggest that the transition is first order as a function of Li content in the ground state.

From the refinement of the diffraction data we extracted magnetic moments and spin angles for each sample and temperature. Similar to the 0001 peak intensity, the magnetic moments M, in all samples, which lie in the range of 4 to 4.8 μ_B at 4 K, drop gradually as the samples approach T_N (see Figure 3a). As stated above, Te is not highly electronegative, which leaves the Mn^{2+} ion less than fully quenched. The addition of Li ions introduces charge carriers (electrons) into the MnTe system. Due to the inductive effect, they are mostly shared with the more electronegative Te, meaning there is less pull on the Mn electrons, and a slightly greater electron density will remain around the Mn atoms. Additionally, as this is a volume effect, the charge from the Li atoms is distributed among all Te due to the conducting nature of MnTe instead of only the neighboring atoms. Here, we have fit the temperature dependence of the order parameter in the high-T region (250-300 K) with a simple power law $M = A(T - T_N)^c$, where A and c are fit parameters (presented in Supplementary Table 2[58]). c is on the order of 0.32 in each compound, as expected in a 3D Heisenberg antiferromagnetic system. Each sample exhibits a constant angle between the spin and the c-axis from 4.2 to ~250 K, above which, in the Li-doped samples, the angle drops off and rapidly approaches the ab-plane, see Figure 3b.

Magnetic Anisotropy Model

To illustrate the spin reorientation upon approaching T_N in Figure 3b, we assume the spin anisotropy energy of the Mn ions take the form $E/N = K_2 M(T)^2 \sin^2\theta - K_4 M(T)^4 \sin^4\theta$, assuming K_4 increases with doping. At 0% Li, K_4 is small and the minimum energy is at $E = 0$ with $\theta = 0$. With increased doping, the energy will dip below zero, so that $1/N dE/d\theta = 2K_2 M(T)^2 \cos\theta \sin\theta - 4K_4 M(T)^4 \cos\theta \sin^3\theta$. Here, the minimum at $\theta = \pi/2$ occurs when $E/N = K_2 M(T)^2 - K_4 M(T)^4 < 0$ or $K_4 M(T)^2/K_2 > 1$. If this condition is barely satisfied upon doping (which increases K_4), then as T approaches T_N, $M(T)$ will decrease, the condition will fail to hold, and the minimum energy will be at $\theta = 0$. The maximum energy $E/N = K_2 M(T)^2/4K_4$ exists where $dE/d\theta = 0$ at $\sin^2\theta = K_2/2K_4 M(T)^2$.

DFT Calculations

We have also calculated the magnetic anisotropy within the antiferromagnetic ground state at 0 K. Contrary to previous reports,[44] we find uniaxial behavior, i.e. orientation of the moments along the c axis, even for pure MnTe. This suggests a possible spin tran-
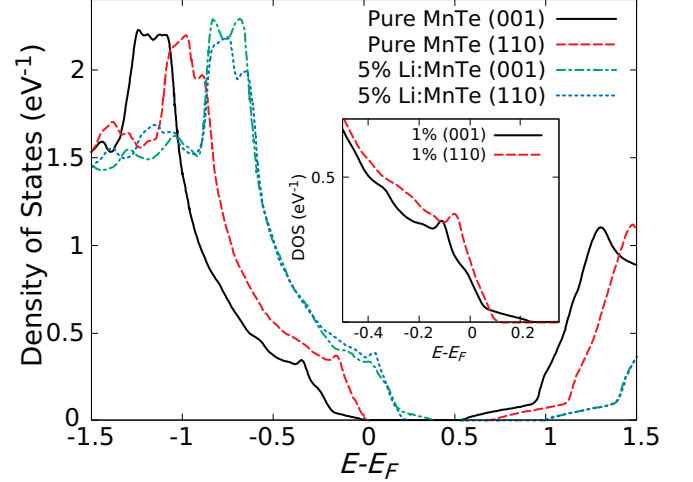

FIG. 4: Total DOS for pure and 5% Li-doped MnTe. (Inset) Magnified total DOS for 1% Li-doped MnTe.

sition at low temperature, similar to that observed in the isostructural material MnBi[68]. The disagreement between these results hints at two competing magnetic ground states in MnTe, one where the easy-axis is in-plane and another uniaxial. With Li alloying within the virtual crystal approximation (VCA), the anisotropy becomes quite large (comparable to that of the permanent magnet $Nd_2Fe_{14}B$). While the VCA can overstate the anisotropy, due primarily to its understatement of the effects of disorder in smearing out near-E_F electronic structure, it generally leads to the correct sign, and indicates that more strongly uniaxial behavior takes place with Li doping.

The significant dependence of the calculated DOS, and in particular the Fermi level, on both moment orientation and Li concentration is consistent with the substantial dependence of the first anisotropy constant K_1 on Li doping. Here, K_1 represents the energy difference, on a volumetric basis, between the (110) and (001) moment configurations. At 0% Li, $K_1 = 0.59$ MJ/m^3, which increases to 2.63 and 4.38 MJ/m^3 at 1% and 5% Li, respectively. As the magnetic anisotropy energy (MAE) is essentially given by the difference of the respective sums of the energy-weighted DOS up to E_F, it is sensible that an orientation-dependent DOS would lead to considerable MAE.

In our DFT calculations, we find that the band gap in pure MnTe is 0.55 eV for the (001) orientation and 0.72 eV for (110). Both are understated relative to experimental data, but the key fact is that the band gap difference is ~170 meV, which should persist even in more sophisticated approaches. The band gap and near-gap electronic structure thus have a substantial dependence on moment orientation, despite finding only a small magnetic anisotropy.

The shape of the calculated density-of-states (DOS)

curves differs significantly depending on spin orientation and Li content, see Figure 4. Additionally, the E_F values in the 1% Li:MnTe differ significantly between orientations.

Calculations of the dipolar anisotropy energy for MnTe for the 5% Li-alloyed case find this energy, for the (001) and (110) orientations, respectively, to be 0.166 and -0.084 MJ/m^3, for a relative contribution of -0.25 MJ/m^3 (the convention being that negative values favor planar alignment). This is more than an order of magnitude smaller than the calculated magnetocrystalline anisotropy for this case, so that addition of the dipolar anisotropy does not affect the moment orientation, or our finding of a planar-to-uniaxial transition resulting from Li doping.

At low doping, resistivity should greatly depend on moment direction. The Li-doping creating a finite DOS at the Fermi level, which changes the material from insulating to metallic and affords good thermoelectric properties[16]. Thus, in the intrinsic regime a $\sim$170 meV difference in band gap yields a factor of $\sim$25 difference in resistivity at 300 K, indicating a potential use for spintronic applications.

In addition, there are thermodynamic effects relevant at larger dopings. The specific heat coefficient, γ, for 1% Li doping is 3.05 mJ/mol-K^2 for the (110) orientation and 2.03 for (001). At 300 K this is a difference of 0.3 J/mol-K (neglecting the temperature dependence of magnetism), or about 0.6% of $3R$. Thus, switching the spin orientation under field will affect thermal response, and should be possible to observe.

CONCLUSION

In this work, we examined the canting of spins from the in-plane orientation in MnTe to axial in Li-doped MnTe. Minimal doping ($\leq$0.3% Li) is required to cant the Mn spins almost completely towards the axial orientation. By 5% Li, the spins are essentially axial. Additionally, the axial anisotropy dominates up to $\sim$250 K before canting back towards the planar orientation upon heating towards the Néel temperature, which is in line with our model of the spin anisotropy.

DFT calculations support the change in magnetic anisotropy with Li doping and indicate and identify the shift in Fermi level as a driving mechanism. However, reaching a level of fine control of the spin orientations will require additional work. An electronic structure which is strongly dependent on moment orientation is expected to host topological transitions due to the competing temperature-dependent energetics of (1) the magnetic ordering energy, (2) the magnetocrystalline energy, and (3) the distinct free energy differences (i.e., specific heat-related) associated with an orientation-dependent $N(E_F)$. Points (2) and (3) are both substantially doping-

dependent in addition, yielding additional complexity.

While the reorientation here involves Li, it is likely that other charge-carrier dopants or strain will produce a similar effect. The extreme sensitivity to doping promises to open new avenues of spintronics and transport research in antiferromagnetic semiconductors such as MnTe. This effect could potentially be applied to layered materials such as the topological insulator MnBi$_2$Te$_4$. Such van der Waals heterostructures could benefit greatly from the ability to easily reorient spins by shifting the Fermi-level.

[1] A. Brataas, A. D. Kent, and H. Ohno, Nat. Mater. **11**, 372 (2012).
[2] C. Chappert, A. Fert, and F. N. Van Dau, Nat. Mater. **6**, 813 (2007).
[3] A. D. Kent and D. C. Worledge, Nat. Nanotechnol. **10**, 187 (2015).
[4] V. Baltz, A. Manchon, M. Tsoi, T. Moriyama, T. Ono, and Y. Tserkovnyak, Rev. Mod. Phys. **90**, 015005 (2018).
[5] C. Song, Y. You, X. Chen, X. Zhou, Y. Wang, and F. Pan, Nanotechnology **29**, 112001 (2018).
[6] I. J. Park, T. Lee, P. Das, B. Debnath, G. P. Carman, and R. K. Lake, Appl. Phys. Lett. **114**, 142403 (2019).
[7] Z. Zhang, E. Liu, W. Zhang, P. K. J. Wong, Z. Xu, F. Hu, X. Li, J. Tang, A. T. S. Wee, and F. Xu, ACS Appl. Mater. Interfaces **11**, 8258 (2019).
[8] A. Boussendel, N. Baadji, A. Haroun, H. Dreyssé, and M. Alouani, Phys. Rev. B **81**, 184432 (2010).
[9] M. Ślezak, T. Ślezak, P. Dróżdż, B. Matlak, K. Matlak, A. Kozioł-Rachwał, M. Zając, and J. Korecki, Sci. Rep.

9, 889 (2019).

[10] M. B. Jungfleisch, W. Zhang, and A. Hoffmann, Phys. Lett. A **382**, 865 (2018).

[11] S. J. Yuan, Y. M. Cao, L. Li, T. F. Qi, S. X. Cao, J. C. Zhang, L. E. DeLong, and G. Cao, J. Appl. Phys. **114**, 113909 (2013).

[12] M. de Souza, J. da Silva, and L. Silva, J. Magn. Magn. Mater. **421**, 184 (2017).

[13] C. Ferrer-Roca, A. Segura, C. Reig, and V. Muñoz, Phys. Rev. B **61**, 13679 (2000).

[14] K. Walther, Solid State Commun. **5**, 399 (1967).

[15] J. D. Wasscher and C. Haas, Phys. Lett. **8**, 302 (1964).

[16] Y. Zheng, T. Lu, M. M. H. Polash, M. Rasoulianborou-jeni, N. Liu, M. E. Manley, Y. Deng, P. J. Sun, X. L. Chen, R. P. Hermann, et al., Sci. Adv. **5**, eaat9461 (2019).

[17] S. M. Wu, J. E. Pearson, and A. Bhattacharya, Phys. Rev. Lett. **114**, 186602 (2015).

[18] K. Uchida, S. Takahashi, K. Harii, J. Ieda, W. Koshibae, K. Ando, S. Maekawa, and E. Saitoh, Nature **455**, 778 (2008).

[19] C. M. Jaworski, J. Yang, S. Mack, D. D. Awschalom, J. P. Heremans, and R. C. Myers, Nat. Mater. **9**, 898 (2010).

[20] P. Gorai, P. Parilla, E. S. Toberer, and V. Stevanović, Chem. Mater. **27**, 6213 (2015).

[21] Z. Li, J.-F. Dong, F.-H. Sun, S. Hirono, and J.-F. Li, Chem. Mater. **29**, 7378 (2017).

[22] Z. Zhou, J. Yang, Q. Jiang, J. Xin, S. Li, X. Wang, X. Lin, R. Chen, A. Basit, and Q. Chen, Chem. Mater. **31**, 3491 (2019).

[23] T. Jungwirth, X. Marti, P. Wadley, and J. Wunderlich, Nat. Nanotechnol. **11**, 231 (2016).

[24] L. Li, H. Li, J. Li, H. Wu, L. Yang, W. Zhang, and H. Chang, Chem. Mater. **33**, 338 (2021).

[25] Q. Lian, L. Zhou, J. Zhang, H. Wu, W. Bai, J. Yang, Y. Zhang, R. Qi, R. Huang, X. Tang, et al., ACS Appl. Nano Mater. **3**, 12046 (2020).

[26] H. Reichlová, D. Kriegner, V. Holý, K. Olejník, V. Novák, M. Yamada, K. Miura, S. Ogawa, H. Takahashi, T. Jungwirth, et al., Phys. Rev. B **92**, 165424 (2015).

[27] P. Wadley, B. Howells, J. Železný, C. Andrews, V. Hills, R. P. Campion, V. Novák, K. Olejník, F. Maccherozzi, S. S. Dhesi, et al., Science **351**, 587 (2016).

[28] X. Marti, I. Fina, C. Frontera, J. Liu, P. Wadley, Q. He, R. J. Paull, J. D. Clarkson, J. Kudrnovský, I. Turek, et al., Nat. Mater. **13**, 367 (2014).

[29] D. Kriegner, K. Výborný, K. Olejník, H. Reichlová, V. Novák, X. Marti, J. Gazquez, V. Saidl, P. Němec, V. V. Volobuev, et al., Nat. Commun. **7**, 11623 (2016).

[30] A. J. Lee, S. Guo, A. S. Ahmed, and F. Yang, Phys. Rev. B **102**, 174434 (2020).

[31] M. S. Wörnle, P. Welter, M. Giraldo, T. Lottermoser, M. Fiebig, P. Gambardella, and C. L. Degen, Phys. Rev. B **103**, 094426 (2021).

[32] A. Zeugner, F. Nietschke, A. U. B. Wolter, S. Gaß, R. C. Vidal, T. R. F. Peixoto, D. Pohl, C. Damm, A. Lubk, R. Hentrich, et al., Chem. Mater. **31**, 2795 (2019).

[33] F. Hou, Q. Yao, C.-S. Zhou, X.-M. Ma, M. Han, Y.-J. Hao, X. Wu, Y. Zhang, H. Sun, C. Liu, et al., ACS Nano **14**, 11262 (2020).

[34] Y. Deng, Y. Yu, M. Z. Shi, Z. Guo, Z. X. Wang, X. H. Chen, and Y. Zhang, Science **367**, 895 (2020).

[35] H. Li, S. Liu, C. Liu, J. Zhang, Y. Xu, R. Yu, Y. Wu, Y. Zhang, and S. Fan, Phys. Chem. Chem. Phys. **22**, 556 (2020).

[36] D. Ovchinnikov, X. Huang, Z. Lin, Z. Fei, J. Cai, T. Song, M. He, Q. Jiang, C. Wang, H. Li, et al., Nano Lett. **21**, 2544 (2021).

[37] K. He, npj Quantum Mater. **5**, 90 (2020).

[38] M.-H. Du, J. Yan, V. R. Cooper, and M. Eisenbach, Adv. Funct. Mater. **31**, 2006516 (2021).

[39] Y. Liu, L.-L. Wang, Q. Zheng, Z. Huang, X. Wang, M. Chi, Y. Wu, B. C. Chakoumakos, M. A. McGuire, B. C. Sales, et al., Phys. Rev. X **11**, 021033 (2021).

[40] J.-Q. Yan, S. Okamoto, M. A. McGuire, A. F. May, R. J. McQueeney, and B. C. Sales, Phys. Rev. B **100**, 104409 (2019).

[41] Q. L. He, G. Yin, A. J. Grutter, L. Pan, X. Che, G. Yu, D. A. Gilbert, S. M. Disseler, Y. Liu, P. Shafer, et al., Nat. Commun. **9**, 2767 (2018).

[42] W. Szuszkiewicz, E. Dynowska, B. Witkowska, and B. Hennion, Phys. Rev. B **73**, 104403 (2006).

[43] Y. H. N. Kunitomi and S. Anzai, J. Phys. Fran **25**, 568 (1964).

[44] D. Kriegner, H. Reichlova, J. Grenzer, W. Schmidt, E. Ressouche, J. Godinho, T. Wagner, S. Y. Martin, A. B. Shick, V. V. Volobuev, et al., Phys. Rev. B **96**, 214418 (2017).

[45] J.-Q. Yan, Q. Zhang, T. Heitmann, Z. Huang, K. Y. Chen, J.-G. Cheng, W. Wu, D. Vaknin, B. C. Sales, and R. J. McQueeney, Phys. Rev. Mater. **3**, 064202 (2019).

[46] M. Krause and F. Bechstedt, J. Supercond. Nov. Magn. **26**, 1963 (2013).

[47] S.-H. Wei and A. Zunger, Phys. Rev. B **35**, 2340 (1987).

[48] S. Mu, R. P. Hermann, S. Gorsse, H. Zhao, M. E. Manley, R. S. Fishman, and L. Lindsay, Phys. Rev. Mater. **3**, 025403 (2019).

[49] S. Y. Park, D. S. Kim, Y. Liu, J. Hwang, Y. Kim, W. Kim, J.-Y. Kim, C. Petrovic, C. Hwang, S.-K. Mo, et al., Nano Lett. **20**, 95 (2020).

[50] W. R. Meier, J. Yan, M. A. McGuire, X. Wang, A. D. Christianson, and B. C. Sales, Phys. Rev. B **100**, 184421 (2019).

[51] H. N. Li, J. W. Huang, L. X. Xiao, L. P. Peng, Y. Y. Wu, G. H. Du, Z. W. Ouyang, B. R. Chen, and Z. C. Xia, J. Appl. Phys. **111**, 083913 (2012).

[52] X. Liu, Z. Jin, S. Zhang, K. Zhang, W. Zhao, K. Xu, X. Lin, Z. Cheng, S. Cao, and G. Ma, J. Phys. D Appl. Phys. **51**, 024001 (2017).

[53] U. Welp, A. Berger, V. K. Vlasko-Vlasov, H. You, K. E. Gray, and J. F. Mitchell, J. Appl. Phys. **89**, 6621 (2001).

[54] Z. Ma, G. Liu, W. Gao, Y. Liu, L. Xie, X. He, L. Liu, Y. Li, and H. Zhang, RSC Adv. **8**, 33487 (2018).

[55] Y. Hu, C.-W. Chen, H. Cao, F. Makhmudov, J. H. Grebenkemper, M. N. Abdusalyamova, E. Morosan, and S. M. Kauzlarich, J. Am. Chem. Soc. **138**, 12422 (2016).

[56] J. Kim, S.-H. Jhi, and R. Wu, Nano Lett. **16**, 6656 (2016).

[57] A. J. Panson and W. D. Johnston, J. Inorg. Nucl. Chem. **26**, 705 (1964).

[58] See Supplemental Material at [URL will be inserted by publisher] for figures for the magnetic susceptibility of pure and Li-doped MnTe, lattice parameters at 4 and 290 K as a function of Li content, and relative lattice parameters with fits. There are tables of the fit parameters of the power law fit of the magnetic moments, basis

vectors of the P63/mmc space group with propagation vector k = (000) and fit parameters for the 3rd-order polynomial fit of the relative lattice parameters. Lastly, there is a discussion of the nominally 3% Li sample, including figures of the magnetic structure, spin angle, and a comparison of the magnetic peak intensity at ARCS and HB-2A.

[59] J. Efrem D'Sa, P. Bhobe, K. Priolkar, A. Das, S. Paranjpe, R. Prabhu, and P. Sarode, J. Magn. Magn. Mater. **285**, 267 (2005).

[60] S. Calder, K. An, R. Boehler, C. R. Dela Cruz, M. D. Frontzek, M. Guthrie, B. Haberl, A. Huq, S. A. J. Kimber, J. Liu, et al., Rev. Sci. Instrum. **89**, 092701 (2018), https://doi.org/10.1063/1.5033906.

[61] A. S. Wills, Physica B Condens. Matter **276-278**, 680 (2000).

[62] J. Perez-Mato, S. Gallego, E. Tasci, L. Elcoro, G. de la Flor, and M. Aroyo, Annu. Rev. Mater. Res. **45**, 217 (2015).

[63] J. Rodríguez-Carvajal, Physica B Condens. Matter **192**, 55 (1993).

[64] D. L. Abernathy, M. B. Stone, M. J. Loguillo, M. S. Lucas, O. Delaire, X. Tang, J. Y. Y. Lin, and B. Fultz, Rev. Sci. Instrum. **83**, 015114 (2012), https://doi.org/10.1063/1.3680104.

[65] A. Floris, S. de Gironcoli, E. K. U. Gross, and M. Cococcioni, Phys. Rev. B **84**, 161102 (2011).

[66] W. L. Roth, Phys. Rev. **110**, 1333 (1958).

[67] A. Wills, J. Phys. IV France **11**, Pr9 (2001).

[68] M. A. McGuire, H. Cao, B. C. Chakoumakos, and B. C. Sales, Phys. Rev. B **90**, 174425 (2014).